Nonlinear Dyn
https://doi.org/10.1007/s11071-022-07632-y

ORIGINAL PAPER

Inner-outer feedback linearization for quadrotor control: two-step design and validation

Luís Martins · **Carlos Cardeira** · **Paulo Oliveira**

Received: 16 September 2021 / Accepted: 3 June 2022

Abstract This paper proposes a novel control architecture for quadrotors that relies twice on the Feedback Linearization technique. The solution comprises a tracking inner-loop resulting from applying the mentioned method to the attitude and altitude dynamics. The horizontal movement, and, thereby, the *zero dynamics*, are stabilized without linearizing nor simplifying it by resorting to the same nonlinear technique. Linear quadratic controllers with integral action are implemented to the resulting chain of integrators of the inner and outer loops. As a result, the inner-loop dynamics asymptotically track the desired attitude and altitude over a broad region of the state-space, and the outer-loop yields a tracking system that is input-to-state stable and exponentially stable in the absence of external inputs. The stability of the proposed inner-outer loop control architecture is studied, leading to the proof of asymptotic stability in an extensive region of the state-space. Trajectory tracking, the capacity to overcome significant deviations on the mass and inertia values, and the robustness to external disturbances are evaluated using a simulation model, in which measurement noise and saturation limits are considered. In addition, comparisons regarding the performance in trajectory tracking of the proposed strategy and the results obtained with similar solutions from the literature are established. Experimental tests were conducted using a commercially available drone, equipped with an Inertial Measurement Unit, a compass, and an altimeter. A motion capture system gives the inertial position of the drone. The results obtained allow the validation of the modeling and control system solution.

Keywords Unmanned aerial vehicle · Nonlinear control system · Feedback control systems · Feedback linearization

L. Martins (✉) · C. Cardeira
IDMEC-Institute of Mechanical Engineering, Instituto Superior Técnico, Universidade de Lisboa, Lisboa, Portugal
e-mail: luis.cunha.martins@tecnico.ulisboa.pt

C. Cardeira
e-mail: carlos.cardeira@tecnico.ulisboa.pt

P. Oliveira
IDMEC-Institute of Mechanical Engineering and ISR-Institute for Systems and Robotics, Instituto Superior Técnico, Universidade de Lisboa, Lisboa, Portugal
e-mail: paulo.j.oliveira@tecnico.ulisboa.pt

1 Introduction

Most recently, due to advances in electronics and manufacturing processes, a miniaturization of the controllers, sensors and processors, without discarding the effectiveness of these components, became a reality. The evolution resulted in the emergence of small configurations of unmanned aerial vehicles. A relevant part of the research conducted on these small-scale UAVs concerns quadrotors. The decrease of the quadrotor cost, which allows the spanning of its use beyond military applications and academic research, in conjunction with its singular characteristics results in being equated

Published online: 29 June 2022

in a panoply of public and civil applications, ranging from search and rescue activities to area monitoring and infrastructure inspection. In furtherance of these small aerial vehicles being autonomous, reliable onboard stabilization and trajectory tracking capabilities are imperative. The number and complexity of the applications of these systems are increasing at an impressive rate. Thus, in order to keep track of this evolution, the control methods applied must be enhanced by aiming better performance and expanded versatility.

The study of the control of quadrotors includes various linear and nonlinear techniques. Several works demonstrate the feasibility of controlling a quadcopter resorting to linear techniques. Notwithstanding this reported success of tackling the control problem with linear techniques, applying nonlinear control methods that consider a more comprehensive model of vehicle dynamics can lead to better performance. In the literature, it is possible to find a variety of nonlinear approaches applied to quadrotors. The majority of these nonlinear strategies relies, for instance, on sliding mode [1–4], backstepping [1,5–7] or model predictive control [8].

A different method commonly considered that has also attracted research interest throughout the years is Feedback Linearization. Freddi et al. used feedback linearization to design a double loop control structure capable of performing not only trajectory tracking but also roll and pitch control in the event of a rotor failure [9]. The simulation tests highlight this capacity of the fault tolerant controller proposed. A distinct two-loop architecture using feedback linearization is proposed in [10]. In the referred work, the attitude of the quadcopter only implicitly appears in the transformation matrix and is not a controlled state. The aerial vehicle proved to fly with good accuracy since the control errors obtained in hovering tests are within 3 cm for all Cartesian coordinates. In [11], a single-loop controller for path following relying on feedback linearization with input dynamic extension is presented. The simulation results validate the strategy. Bonna et al., in [12], proposed a similar single-loop control solution based on feedback linearization with dynamic extension. The resulting input-output linearized model is controlled by resorting to the LQR technique. The proposed dynamic nonlinear control law was studied in simulation. Vallejo-Alarcon, in [13], assumed simplifying conditions regarding the attitude and position dynamics to develop a control scheme that combines the feedback linearization and backstepping techniques, having presented experimental results. In [14], Aboudonia et al. designed a feedback linearization controller that incorporates a disturbance observer. The authors assessed the impact of the neglected nonlinear dynamics through a simulation study.

This work presents a novel nonlinear control architecture for quadrotors. The control problem is addressed without simplifications or approximations of the underlying differential equations of the dynamic model, which captures the fundamental dynamics of the vehicle. This constitutes one of the main differences compared with some works based on feedback linearization found in the literature (cf. [9,13–15]), in which simplifying assumptions and approximations are considered. Further, the authors also discuss the impact of the coupling between the two resulting tracking systems and prove the stability of the interconnected system. The solution was tested in simulation and experimentally validated resorting to an off-the-shelf quadcopter. The reconstruction of the state-variables that are not directly available through sensors, namely the velocity and the Euler angles, is performed resorting to Kalman Filters and a nonlinear attitude filter, respectively. An inner-outer loop structure is proposed as the control solution, where the innermost loop is responsible for the attitude and altitude control, and the outermost solves the horizontal positioning control. In both loops an integral action is present. Linear Quadratic Regulator and Feedback Linearization methods are considered to tackle the control problem. Although the use of the Euler angles representation constitutes a hindrance in attaining global asymptotic stability and state-of-the-art works demonstrate the feasibility of achieving global attitude tracking by resorting to a quaternion-based control, for instance ([16]), for practical reasons, the Euler angle parameterization is explored in this work due to its intuitiveness. In this direction, the resulting control architecture is regionally stable. Notwithstanding, the proven region of stability of the architecture is more than sufficient for most applications with quadrotors since it completely encloses the flight envelope required in non-acrobatic flights.

The main contribution of this work is a novel control structure that relies twice on the nonlinear technique Feedback Linearization in combination with LQR control with integral action. To the best of the authors' knowledge, there are no solutions for quadrotor control in the literature in which the Feedback Linearize-

tion technique is applied simultaneously for position and attitude control in a double-loop architecture. The outer-loop controller governs the horizontal movement dynamics and yields a tracking system that is input-to-state stable and exponentially stable in the absence of external inputs. The inner-loop tackles the attitude and altitude control problems and the resulting closed-loop tracking system is asymptotically stable for $|\varphi| < \frac{\pi}{2}$ and $|\theta| < \frac{\pi}{2}$. The proposed strategy has integral action embedded in both loops to deal more effectively with constant disturbances and parameter uncertainties. The interconnection between the inner and outer loops tracking systems is studied by capitalizing on the input-to-state stability property of the horizontal movement tracking dynamics. As a result, the control strategy transforms the quadrotor dynamics into a double-loop architecture tracking system that is asymptotic stable for $|\varphi| < \frac{\pi}{2}$ and $|\theta| < \frac{\pi}{2}$. The proposed strategy proposed results from deepening the authors' former works, in which a conventional linear method, [17], and a combination between linear methods and Feedback Linearization, [15], were considered. When compared to the latter work, the outer-loop control law devised, based on Feedback Linearization, results in a broader region of proved asymptotic stability.

The novel control solution overcame extreme model inaccuracies and a constant external force in simulation without deteriorating its performance. In detail, the authors considered four different scenarios, arising from combinations of variations of $\pm 50\%$ of the mass value with variations of $+300\%$ and -75% of the inertia values, under the influence of an external force of 1 N. The promising results evidence the importance of the integral action. Further, in a second simulation test, in which the authors evaluate the trajectory tracking capacity, the control solution outperformed similar strategies based on Feedback Linearization from the literature. In experimental tests conducted with a commercially available vehicle, the proposed solution successfully followed a predefined trajectory. To expand the evaluation, the authors studied the behavior of the solution when performing aggressive maneuvers and when subjected to considerable constant perturbations. To this end, an offset of $-35°$ was applied to the pitch reference while the quadrotor was hovering. Despite the significant unexpected constant disturbance and the consequent aggressive maneuver, which solicited the nonlinear dynamics of the quadrotor, the vehicle presents a stable response and returns to the desired position. The experimental results obtained in the two tests validate the approach. Compared to the minority of works related to Feedback Linearization that validate the respective solution with an actual vehicle, the experimental study presented in this manuscript is more extensive.

Compared to other strategies from literature, the first advantage of the approach stems from applying the Feedback Linearization technique that transforms the attitude and altitude dynamics, which form the inner-loop, and the horizontal movement dynamics, governed by the outer-loop, into linear and decoupled tracking systems formed by chains of integrators. The transformation allows applying the LQR method to compute the feedback gains and, thereby, capitalize on the large stability margins to errors in the loop gain that this linear method offers, namely, gain margin of infinity, gain reduction margin of 1/2, and a minimum phase margin of 60° ([18]). The second advantage is related to the input-to-state stability property of the resulting horizontal movement tracking system. This property is instrumental for studying the interconnection between the two loops and concluding the stability of the resulting architecture. The outer-loop control law devised enables obtaining a more extensive region of proved asymptotic stability when compared with other double-loop architectures from the literature that also rely on the same nonlinear control method [15,19]. The integral action is a crucial element of the solution since it allows dealing more effectively with constant disturbances and significant mismatch of the model parameters, thus, increasing the robustness of the strategy. The simulation and experimental results attained corroborate this idea. In this direction, the inclusion of integral action in both loops is another relevant advantage relative to other strategies based on feedback linearization from the literature. Against single-loop solutions from literature (for instance, [11,12]), the proposed structure has fewer singularities, is computationally less demanding, and does not require estimating position high-order derivatives that are more affected by measurement noise. The disadvantage of the control solution is using the Euler angles representation, which constitutes a clear obstacle in attaining a global result. However, given the valencies previously mentioned and the extensive region of proved asymptotic stability, the novel control architecture proposed by the authors is advantageous with respect with other simi-

lar strategies and can be effectively used in the vast majority of applications with quadrotors.

This manuscript is organized as follows: first, in Sect. 2, the underlying differential equations of the nonlinear model and the computation of the thrust and moments are detailed; next, the control solution design and the proofs of asymptotic stability are presented in Sect. 3; the simulation results obtained with the architecture are displayed and analyzed in Sect. 4; posteriorly, in Sect. 5, the transition to the actual aerial vehicle is addressed through an overview of the quadcopter and its sensors, and the description of the implementation of the controllers and state-estimators; the experimental validation responses are displayed and evaluated in Sect. 6; lastly, in Sect. 7, the manuscript ends with some concluding remarks.

2 Physical model

In this section, the nonlinear model of the UAV based on the Newton-Euler formalism is presented. The model is formulated considering a body and an inertial reference frames, denoted as, respectively, $\{O_n, X_n Y_n Z_n\}$ and $\{O_I, X_I Y_I Z_I\}$. These reference frames are depicted in Fig. 1.The origin of the body-fixed frame $\{B\}$ is coincident with the center of mass of the quadrotor. The formulation of the dynamic model relies on some frequently adopted and perfectly reasonable assumptions: the vehicle is symmetrical and rigid, the motor dynamics are relatively fast and can be neglected, and a lumped parameter describes the relationship between the thrust and yaw moment generated by a rotor in free-air, as discussed by [20].

Let $\mathbf{p} = (x, y, z) \in \mathbb{R}^3$ denote the position vector of the center of mass of the UAV in the inertial frame. Let $\boldsymbol{\eta} = (\varphi, \theta, \psi) \in \mathbb{R}^3$ describe the orientation vector, in terms of Euler angles, of the body-fixed frame with respect to the inertial frame, where φ, θ and ψ are the roll, pitch and yaw angles, respectively. Let $\boldsymbol{\omega} = (p, q, r) \in \mathbb{R}^3$ represent the angular velocity described in the body-fixed reference frame. The rigid body equations of motion of the quadcopter, according to Mahony et al. [21], are given by:

$$m\ddot{p} = -mg\mathbf{e_3} + \mathbf{R}T\mathbf{e_3} \tag{1}$$

$$\mathbf{I}\dot{\boldsymbol{\omega}} = -\boldsymbol{\omega} \times \mathbf{I}\boldsymbol{\omega} + \boldsymbol{\tau} \tag{2}$$

where $\mathbf{I} \in \mathbb{R}^{3\times3}$ corresponds to the diagonal inertia matrix described in the body fixed-frame, $m \in \mathbb{R}$ is the

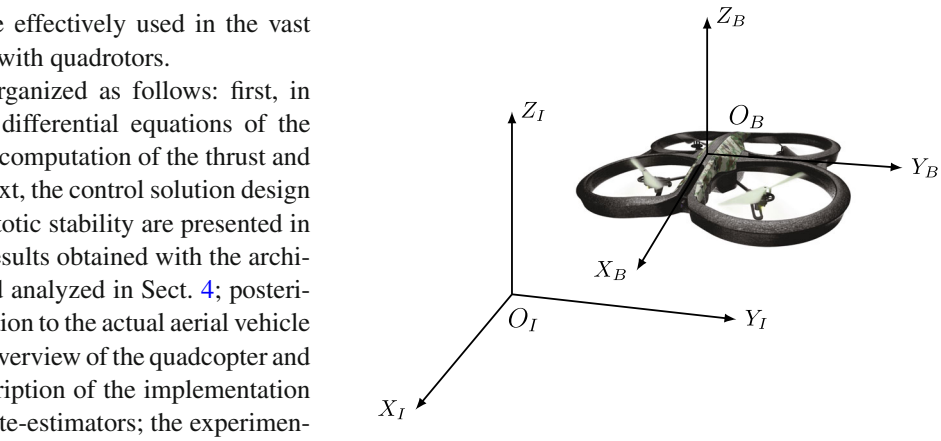

Fig. 1 Reference frames in which the nonlinear dynamics are described

total mass of the quadrotor, $g \in \mathbb{R}$ denotes the gravity acceleration, $T \in \mathbb{R}$ and $\boldsymbol{\tau} = (\tau_\varphi, \tau_\theta, \tau_\psi) \in \mathbb{R}^3$ denote, respectively, the total thrust and moments applied to the UAV airframe by the aerodynamics of the rotors, both described in the body-fixed reference frame, $\mathbf{e_3} \in \mathbb{R}^3$ is a vector of zeros except for the 3rd entry which is 1, and $\mathbf{R} \in \mathrm{SO}(3)$ is the rotation matrix from the body-fixed to the inertial reference frame. The Euler angles follow the sequence of rotation Z-Y-X that is described in [22].

$$\dot{\boldsymbol{\eta}} = \mathbf{T}(\boldsymbol{\eta})\,\boldsymbol{\omega} = \begin{bmatrix} 1 & \sin(\varphi)\tan(\theta) & \cos(\varphi)\tan(\theta) \\ 0 & \cos(\varphi) & -\sin(\varphi) \\ 0 & \sin(\varphi)\sec(\theta) & \cos(\varphi)\sec(\theta) \end{bmatrix} \boldsymbol{\omega} \tag{3}$$

According to Leishman [20], the steady-state thrust $T_i \in \mathbb{R}$ and yaw moment $\tau_{\psi_i} \in \mathbb{R}$ generated by a rotor in free air can be related through a lumped parameter model. The parameter, c_i, can be experimentally determined. The roll and pitch moments, $\tau_\varphi \in \mathbb{R}$ and $\tau_\theta \in \mathbb{R}$, result from the generated thrust of the rotor and its arrangement relative to the center of mass of the quadcopter. Hence, the resultant total thrust T and moments τ_φ, τ_θ and τ_ψ are computed through:

$$\begin{bmatrix} T \\ \tau_\varphi \\ \tau_\theta \\ \tau_\psi \end{bmatrix} = \begin{bmatrix} 1 & 1 & 1 & 1 \\ L & -L & -L & L \\ -L & -L & L & L \\ c_1 & -c_2 & c_3 & -c_4 \end{bmatrix} \begin{bmatrix} T_1 \\ T_2 \\ T_3 \\ T_4 \end{bmatrix} \tag{4}$$

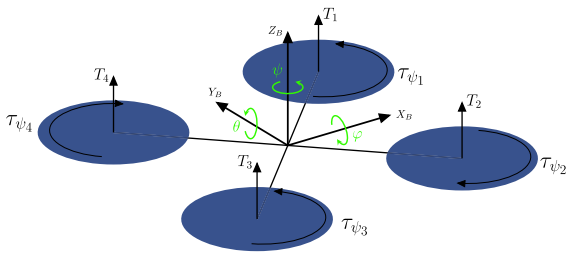

Fig. 2 Schematic representation of the Euler angles and forces and moments generated by each rotor

In Fig. 2, the forces and yaw moments generated by each rotor, the direction of rotation of each propeller, the dimension L and the Euler angles are schematically represented.

Let $\mathbf{x} \in \mathbb{R}^{12}$ denote the state-variables vector

$$\mathbf{x} = [x \;\; y \;\; z \;\; \varphi \;\; \theta \;\; \psi \;\; \dot{x} \;\; \dot{y} \;\; \dot{z} \;\; p \;\; q \;\; r]^\top \tag{5}$$

and let $\mathbf{u} \in \mathbb{R}^4$ represent the input vector

$$\mathbf{u} = \begin{bmatrix} T & \tau_\varphi & \tau_\theta & \tau_\psi \end{bmatrix}^\top \tag{6}$$

Then, the quadcopter dynamics can be written in the compact form

$$\dot{\mathbf{x}} = \begin{bmatrix} \dot{\mathbf{p}} \\ \mathbf{T}(\boldsymbol{\eta})\,\boldsymbol{\omega} \\ -g\mathbf{e_3} \\ \mathbf{I}^{-1}(\mathbf{I}\boldsymbol{\omega} \times \boldsymbol{\omega}) \end{bmatrix} + \begin{bmatrix} \mathbf{0}_{6\times1} & \mathbf{0}_{6\times3} \\ \frac{1}{m}\mathbf{R}\mathbf{e_3} & \mathbf{0}_{3\times3} \\ \mathbf{0}_{3\times1} & \mathbf{I}^{-1} \end{bmatrix} \mathbf{u} \tag{7}$$

with $i = 1, 2, 3$.

3 Control

To tackle the control problem, an inner-outer loop structure is considered in which static-state feedback linearization is applied not only to the inner loop dynamics, formed by the attitude and altitude equations, but also to the *zero dynamics* through an outer-loop that generates the references for the roll and pitch angles. The solution proposed in this paper addresses the intricate problem of the horizontal movement and, thereby the *zero dynamics*, without linearizing nor simplifying it. Let the desired trajectory be defined, for $t \geq 0$, by the map

$$\mathbf{r}(t) := \left(\mathbf{p_d}(t), \dot{\mathbf{p}}_d(t), \ddot{\mathbf{p}}_d(t), \psi_d(t), \dot{\psi}_d(t), \ddot{\psi}_d(t)\right), \tag{8}$$

which encompasses the desired position, $\mathbf{p_d}$, and yaw angle, ψ_d, and the respective derivatives. The control objective is to design T and $\boldsymbol{\tau}$ such that the desired trajectory is successfully tracked.

Feedback Linearization consists in a nonlinear control approach that aims to algebraically transform nonlinear dynamics of systems, through nonlinear change of coordinates and nonlinear state feedback, into a model that is linear in the new set of coordinates. The linear model produced is an exact representation of the original nonlinear model over a large set of operating points [23]. Given a nonlinear system of the form:

$$\dot{\mathbf{x}} = \mathbf{f}(\mathbf{x}) + \mathbf{g}(\mathbf{x})\,\mathbf{u} \tag{9}$$

$$\mathbf{y} = \mathbf{h}(\mathbf{x}) \tag{10}$$

with the state vector $\mathbf{x} \in \mathbb{R}^{\mathrm{n}}$ and where $\mathbf{f}(\mathbf{x}) \in \mathbb{R}^{\mathrm{n}}$ and $\mathbf{h}(\mathbf{x}) \in \mathbb{R}^{\mathrm{m}}$ are vectors of sufficiently smooth nonlinear functions and $\mathbf{g}(\mathbf{x}) \in \mathbb{R}^{\mathrm{n}\times\mathrm{m}}$ is a matrix of sufficiently smooth nonlinear functions. From [24, Lemma 5.2.1], assume the former nonlinear system verifies the conditions therein stated, the system can be modified into a fully linear and decoupled controllable system through the application of the following *diffeomorphism* $\boldsymbol{\Phi}(\mathbf{x}) \in \mathbb{R}^{\mathrm{n}}$:

$$\boldsymbol{\xi}_{j,k} = \boldsymbol{\phi}_{j,k}(\mathbf{x}) = \mathcal{L}_{\mathbf{f}}^{\mathbf{k}-\mathbf{1}}\mathbf{h}_j(\mathbf{x}) \tag{11}$$

with $k \in \{1, ..., \mathbf{r}_j\}$, $j \in \{1, ..., \mathrm{m}\}$ and where $\mathcal{L}$ denotes the Lie Derivative and $\mathbf{r}_j$ represents the relative order, and of the next nonlinear static state feedback control law

$$\mathbf{u} = -\Lambda^{-1}(\mathbf{x})\,\mathbf{b}(\mathbf{x}) + \Lambda^{-1}(\mathbf{x})\,\mathbf{v} \tag{12}$$

where $\mathbf{v} \in \mathbb{R}^{\mathrm{m}}$ denote the transformed input variables vector, the *decoupling matrix* $\Lambda(\mathbf{x}) \in \mathbb{R}^{\mathrm{m}\times\mathrm{m}}$ is defined as

$$\Lambda(\mathbf{x}) = \begin{bmatrix} \mathcal{L}_{\mathbf{g}_1}\mathcal{L}_{\mathbf{f}}^{\mathbf{r_1}-\mathbf{1}}\mathbf{h}_1(\mathbf{x}) & \cdots & \mathcal{L}_{\mathbf{g}_\mathrm{m}}\mathcal{L}_{\mathbf{f}}^{\mathbf{r_1}-\mathbf{1}}\mathbf{h}_1(\mathbf{x}) \\ \vdots & \ddots & \vdots \\ \mathcal{L}_{\mathbf{g}_1}\mathcal{L}_{\mathbf{f}}^{\mathbf{r_m}-\mathbf{1}}\mathbf{h}_\mathrm{m}(\mathbf{x}) & \cdots & \mathcal{L}_{\mathbf{g}_\mathrm{m}}\mathcal{L}_{\mathbf{f}}^{\mathbf{r_m}-\mathbf{1}}\mathbf{h}_\mathrm{m}(\mathbf{x}) \end{bmatrix} \tag{13}$$

and $\mathbf{b}(\mathbf{x}) \in \mathbb{R}^{\mathrm{m}}$ is given by

$$\mathbf{b}(\mathbf{x}) = \begin{bmatrix} \mathcal{L}_{\mathbf{f}}^{\mathbf{r_1}} \mathbf{h}_1(\mathbf{x}) & \dots & \mathcal{L}_{\mathbf{f}}^{\mathbf{r_m}} \mathbf{h}_{\mathrm{m}}(\mathbf{x}) \end{bmatrix}^{\top} \tag{14}$$

It is clear that the *decoupling matrix* $\Lambda(\mathbf{x})$ is required to be nonsingular. After applying the input-output feedback linearization, the input-output model is linear in the new set of coordinates and is formed by a set of m chains of $\mathbf{r}_j$ integrators with inputs $\mathbf{v}_j$ described by:

$$\mathbf{v}_j = \mathcal{L}_{\mathbf{f}}^{\mathbf{r_j}} \mathbf{h}_j(\mathbf{x}) + \sum_{i=1}^{m} \mathcal{L}_{\mathbf{g}_i} \mathcal{L}_{\mathbf{f}}^{\mathbf{r_j}-\mathbf{1}} \mathbf{h}_j(\mathbf{x}) \mathbf{u}_i = \dot{\boldsymbol{\xi}}_{j,\mathbf{r}_j} \tag{15}$$

3.1 Attitude and altitude control

Let $\mathbf{x_{in}} \in \mathbb{R}^8$ denote the vector of state-variables of the inner dynamics

$$\mathbf{x_{in}} = \begin{bmatrix} z & \varphi & \theta & \psi & \dot{z} & p & q & r \end{bmatrix}^{\top} \tag{16}$$

and $\mathbf{u_{in}} \in \mathbb{R}^4$ describe the vector of inputs of the system

$$\mathbf{u_{in}} = \begin{bmatrix} T & \tau_{\varphi} & \tau_{\theta} & \tau_{\psi} \end{bmatrix}^{\top} \tag{17}$$

By recalling the nonlinear model presented in (7), it is possible to express the inner loop dynamics with the form described in (9) and (10):

$$\dot{\mathbf{x}}_{in} = \begin{bmatrix} \dot{z} \\ \mathbf{T}(\boldsymbol{\eta})\,\boldsymbol{\omega} \\ -g \\ \mathbf{I}^{-1}(\mathbf{I}\boldsymbol{\omega} \times \boldsymbol{\omega}) \end{bmatrix} + \begin{bmatrix} \mathbf{0}_{4\times 1} & \mathbf{0}_{4\times 3} \\ \frac{c_\varphi c_\theta}{m} & \mathbf{0}_{1\times 3} \\ \mathbf{0}_{3\times 1} & \mathbf{I}^{-1} \end{bmatrix} \mathbf{u_{in}} \tag{18}$$

$$\mathbf{y_{in}} = \begin{bmatrix} z & \varphi & \theta & \psi \end{bmatrix}^{\top} \tag{19}$$

In the majority of the works found in the literature, the inner-loop governs the attitude dynamics. In this work, this loop also encapsulates the altitude dynamics since this inclusion does not yield additional singularities and provides a straightforward computation of the thrust magnitude required. To tackle the attitude and altitude control problem, the strategy detailed in [15] is applied. First, it follows from [15, Proposition 1] that the inner-loop dynamics described by (18) and (17) with output (19) have a well-defined relative degree vector $\mathbf{r} = \{2, 2, 2, 2\}$ on the set $\left\{\mathbf{x_{in}} \in \mathbb{R}^8 : |\varphi|, |\theta| < \frac{\pi}{2}\right\}$.

In this direction, by resorting to the following static state feedback control law reported in [15]

$$\mathbf{u_{in}} = -\Lambda_{\mathbf{in}}^{-\mathbf{1}}(\mathbf{x_{in}})\,\mathbf{b_{in}}(\mathbf{x_{in}}) + \Lambda_{\mathbf{in}}^{-\mathbf{1}}(\mathbf{x_{in}})\,\mathbf{v_{in}} \tag{20}$$

where

$$\Lambda_{\mathbf{in}}(\mathbf{x_{in}}) = \begin{bmatrix} \frac{c_\theta\, c_\varphi}{m} & 0 & 0 & 0 \\ 0 & \frac{1}{I_x} & \frac{t_\theta\, s_\varphi}{I_y} & \frac{c_\varphi\, t_\theta}{I_z} \\ 0 & 0 & \frac{c_\varphi}{I_y} & -\frac{s_\varphi}{I_z} \\ 0 & 0 & \frac{s_\varphi}{I_y\, c_\theta} & \frac{c_\varphi}{I_z\, c_\theta} \end{bmatrix} \tag{21}$$

with $t_{()}$ being the shorthand form for tangent, the inner dynamics are input-output linearized. The vector $\mathbf{b_{in}}(\mathbf{x_{in}})$ encompasses the terms of the second-order time derivative of the output that are independent of the input. The *local diffeomorphism* (11) originates the following vector of transformed state-variables:

$$\boldsymbol{\xi}_{\mathbf{in}} = \begin{bmatrix} z & \dot{z} & \varphi & \dot{\varphi} & \theta & \dot{\theta} & \psi & \dot{\psi} \end{bmatrix}^{\top} = \boldsymbol{\Phi}(\mathbf{x_{in}}) \tag{22}$$

Consequently, the static state feedback control law in conjunction with the change of coordinates (11) transforms the inner dynamics into four single-input single-output chains of two integrators. In virtue of the resulting dynamics being controllable, decoupled, and linear, the Linear Quadratic Regulator control technique can be applied. An integrator is embedded into the feedback control in furtherance of dealing with the steady-state error and mitigating the effect of perturbations [18]. Let the attitude error $\mathbf{e}_{\boldsymbol{\eta}}$ be defined by $\mathbf{e}_{\boldsymbol{\eta}} = (\boldsymbol{\eta} - \boldsymbol{\eta}_{\mathbf{d}})$, where $\boldsymbol{\eta}_{\mathbf{d}} = (\varphi_d, \theta_d, \psi_d)$, with φ_d and θ_d denoting the desired roll and pitch angles that result from the outer-loop control law, and let $\mathbf{e_p} = (\mathbf{p} - \mathbf{p_d})$ represent the position error. The transformed input vector $\mathbf{v_{in}}$ is defined as follows:

$$\mathbf{v_{in}} = \begin{bmatrix} \mathbf{e_3}^{\top}(-k_{i_z}\dot{\boldsymbol{\zeta}}_{\mathbf{p}} - k_z\mathbf{e_p} - k_{\dot{z}}\dot{\mathbf{e}}_p + \ddot{\mathbf{p}}_d) \\ -\mathbf{K_{i}}_{\boldsymbol{\eta}}\boldsymbol{\zeta}_{\boldsymbol{\eta}} - \mathbf{K}_{\boldsymbol{\eta}}\mathbf{e}_{\boldsymbol{\eta}} - \mathbf{K}_{\dot{\boldsymbol{\eta}}}\dot{\mathbf{e}}_{\boldsymbol{\eta}} + \ddot{\boldsymbol{\eta}}_{\mathbf{d}} \end{bmatrix} \tag{23}$$

where k_{i_z}, k_z, $k_{\dot{z}}$, $\mathbf{K_{i}}_{\boldsymbol{\eta}}$, $\mathbf{K}_{\boldsymbol{\eta}}$, and $\mathbf{K}_{\dot{\boldsymbol{\eta}}}$ are gains that result from the application of the LQR gain computation and $\boldsymbol{\zeta}_{\boldsymbol{\eta}}$ and $\boldsymbol{\zeta}_{\mathbf{p}}$ are integral states satisfying

$$\dot{\boldsymbol{\zeta}}_{\boldsymbol{\eta}} = \mathbf{e}_{\boldsymbol{\eta}}, \quad \dot{\boldsymbol{\zeta}}_{\mathbf{p}} = \mathbf{e_p} \tag{24}$$

The feedback defined in (20) and (23), in combination with the *local diffeomorphism* (22), yields the following altitude and attitude tracking dynamics:

$$\begin{bmatrix} \mathbf{e_3}^\top \ddot{\mathbf{e}}_p \\ \ddot{\mathbf{e}}_\eta \end{bmatrix} = \begin{bmatrix} \mathbf{e_3}^\top (-k_{i_z} \boldsymbol{\zeta}_\mathbf{p} - k_z \mathbf{e_p} - k_{\dot{z}} \dot{\mathbf{e}}_p) \\ -\mathbf{K_{i_\eta}} \boldsymbol{\zeta}_\eta - \mathbf{K}_\eta \mathbf{e}_\eta - \mathbf{K}_{\dot{\eta}} \dot{\mathbf{e}}_\eta \end{bmatrix} \tag{25}$$

The altitude and attitude tracking dynamics are asymptotically stable for all $\mathbf{x_{in}}$ satisfying $|\varphi| < \frac{\pi}{2}$ and $|\theta| < \frac{\pi}{2}$.

3.2 Zero dynamics control

With the inner-loop dynamics stabilized, it is now relevant to determine the *zero dynamics*, by solving the *Problem of Zeroing the Output* [24], and analyze the corresponding internal dynamics of the system described in (7). If $\mathbf{y_{in}} = \mathbf{0}$, then $\boldsymbol{\xi}_\mathbf{in} = \mathbf{0}$ and, considering (15), $\mathbf{v_{in}} = \mathbf{0}$. Given (12), the input vector $\mathbf{u_{in}}$ that solves the *Problem of Zeroing the Output* is computed through:

$$\mathbf{0} = \mathbf{b_{in}}(\mathbf{x_{in}}) + \Lambda_\mathbf{in}(\mathbf{x_{in}})\, \mathbf{u_{in}} \tag{26}$$

The first equation of the system (26) is equivalent to equaling the height second time-derivative to zero. Solving this equation yields:

$$T = mg \tag{27}$$

Taking into account (7) and the former result, the horizontal movement dynamics can be specified through

$$\ddot{x} = g\,(\cos(\varphi)\sin(\theta)\cos(\psi) + \sin(\varphi)\sin(\psi)) \tag{28}$$

$$\ddot{y} = g\,(\cos(\varphi)\sin(\theta)\sin(\psi) - \sin(\varphi)\cos(\psi)) \tag{29}$$

An outer position control loop is required to control these dynamics. By letting $\mathbf{x_{out}} \in \mathbb{R}^4$ denote the vector of state-variables of the outer dynamics

$$\mathbf{x_{out}} = \begin{bmatrix} x & y & \dot{x} & \dot{y} \end{bmatrix}^\top \tag{30}$$

the outer-loop dynamics can be perceived as

$$\dot{\mathbf{x}}_\mathbf{out} = f\,(\mathbf{x_{out}},\ \boldsymbol{\eta}) \tag{31}$$

Since the translational control dictates the roll and pitch angle required to track the desired trajectory, let $\mathbf{u_{out}} \in \mathbb{R}^2$ describe the vector of inputs of the outermost loop

$$\mathbf{u_{out}} = (\cos(\varphi)\sin(\theta), \sin(\varphi)) \tag{32}$$

Given (28) and (29), the outer-loop dynamics can be described with the form described in (9) and (10):

$$\dot{\mathbf{x}}_{out} = \begin{bmatrix} \mathbf{0} & \boldsymbol{I}_2 \\ \mathbf{0} & \mathbf{0} \end{bmatrix} \mathbf{x_{out}} + g \begin{bmatrix} \mathbf{0} & \mathbf{0} \\ \cos\psi & \sin\psi \\ \sin\psi & -\cos\psi \end{bmatrix} \mathbf{u_{out}} \tag{33}$$

$$\mathbf{y_{out}} = \begin{bmatrix} x & y \end{bmatrix}^\top \tag{34}$$

Lemma 1 *The outer-loop dynamics described by* (33) *and* (32) *with output* (34) *have a well-defined relative degree vector* $\{\mathbf{r}_1, \mathbf{r}_2\} = \{2, 2\}$ *for any* $\mathbf{x_{out}}$.

Proof Following the reasoning of the proof of [15, Proposition 1], it is evident that the first time derivative of the output vector $\mathbf{y_{out}}$ is independent of the inputs. From the second time derivative of the output vector, the following *decoupling matrix* is obtained:

$$\Lambda_\mathbf{out}(\psi) = \begin{bmatrix} g\cos(\psi) & g\sin(\psi) \\ g\sin(\psi) & -g\cos(\psi) \end{bmatrix} \tag{35}$$

whose determinant is defined by

$$\det(\Lambda_\mathbf{out}(\psi)) = -g^2 \tag{36}$$

Thereby, the *decoupling matrix* $\Lambda_\mathbf{out}(\psi)$ is invertible for any $\mathbf{x_{out}}$. Furthermore, the first condition is also verified, $\mathcal{L}_{\mathbf{g_i}} \mathcal{L}_\mathbf{f}^\mathbf{k} \mathbf{h}_j(\mathbf{x_{out}}) = \mathbf{0}$ for $i, j \in \{1, 2\}$, $k \in \{0, ..., \mathbf{r}_j - 2\}$. Consequently, the outer-loop dynamics have well-defined relative degree vector at any point $\mathbf{x_{out}}$. □

The sum of the entries of the relative degree vector of the nonlinear system expressed in (33) and (34) is equal to the number of state-variables of the referred system, $\sum_{j=1}^{2} \mathbf{r}_j = 4$. Thus, the outer-loop dynamics are possible to be input-output linearized through the following static state feedback law

$$\mathbf{u_{out}} = \Lambda_\mathbf{out}^{-\mathbf{1}}(\psi)\, \mathbf{v_{out}} \tag{37}$$

Note that, in this case, the coordinates transformation described in (11) yields

$$\boldsymbol{\xi}_\mathbf{out} = \boldsymbol{\Phi}\,(\mathbf{x_{out}}) = \mathbf{x_{out}} \tag{38}$$

As a result of the static state feedback control law, the outer-loop dynamics are now translated into two single-input single-output chains of two integrators. Gi- ven the Brunovsky canonical form, the LQR with integral

action can be applied to each chain by following a procedure similar to the one used for the inner loop. The transformed input variables are given by:

$$\mathbf{v_{out}} = \begin{bmatrix} \mathbf{e_1}^\top(-k_{i_x}\boldsymbol{\zeta}_\mathbf{p} - k_x\mathbf{e_p} - k_{\dot{x}}\dot{\mathbf{e}}_p + \ddot{\mathbf{p}}_d) \\ \mathbf{e_2}^\top(-k_{i_y}\boldsymbol{\zeta}_\mathbf{p} - k_y\mathbf{e_p} - k_{\dot{y}}\dot{\mathbf{e}}_p + \ddot{\mathbf{p}}_d) \end{bmatrix} \tag{39}$$

where $k_{i_x}, k_x, k_{\dot{x}}, k_{i_y}, k_y, k_{\dot{y}}$ are gains resulting from the application of the LQR gain computation. The feedback law defined in (37) and (39) leads to the following tracking system for the zero dynamics

$$\begin{bmatrix} \mathbf{e_1}^\top\ddot{\mathbf{e}}_p \\ \mathbf{e_2}^\top\ddot{\mathbf{e}}_p \end{bmatrix} = \begin{bmatrix} \mathbf{e_1}^\top(-k_{i_x}\boldsymbol{\zeta}_\mathbf{p} - k_x\mathbf{e_p} - k_{\dot{x}}\dot{\mathbf{e}}_p) \\ \mathbf{e_2}^\top(-k_{i_y}\boldsymbol{\zeta}_\mathbf{p} - k_y\mathbf{e_p} - k_{\dot{y}}\dot{\mathbf{e}}_p) \end{bmatrix} \tag{40}$$

Theorem 1 *Let the outer-loop dynamics be described by* (32) *and* (33) *and have its output expressed by* (34)*. The closed-loop tracking system* (40)*, resulting from applying the feedback defined by* (37) *and* (39)*, is regionally exponentially stable.*

Proof From Lemma 1, for the outer-loop dynamics, the noninteracting control problem has solution for all points $(\mathbf{x_{out}}, \boldsymbol{\eta})$. Thereby, applying the control law defined by (37) results in the reduction of the outer-loop dynamics to two chains of two integrators. As a consequence of imposing the feedback defined by (39), the characteristic polynomial of each resulting chain of integrators of the tracking system in closed-loop is Hurwitz and, therefore, the linear state-variables $\boldsymbol{\xi}_\mathbf{out}$ converge exponentially to the desired position trajectory for any initial state $\boldsymbol{\xi}_\mathbf{out}(0)$. Furthermore, from [15, Theorem 3], the Euler angles are asymptotically stabilized provided the condition $|\varphi| < \frac{\pi}{2}$ and $|\theta| < \frac{\pi}{2}$ is satisfied. Once $\boldsymbol{\xi}_\mathbf{out} = \mathbf{x_{out}}$, the horizontal movement tracking dynamics (40) are exponentially stable for all $\mathbf{x_{out}}$ and for all $\boldsymbol{\eta}$ verifying the condition $|\varphi| < \frac{\pi}{2}$ and $|\theta| < \frac{\pi}{2}$. □

The *zero dynamics*, according to the definition presented by Isidori in [24], are obtained by imposing $\boldsymbol{\eta}$ to be identically zero in the outer-loop dynamics. Consequently, the *zero dynamics* are described by

$$\dot{\mathbf{x}}_\mathbf{out} = f(\mathbf{x_{out}}, \mathbf{0}) \tag{41}$$

Corollary 1 *The zero dynamics globally exponentially track the desired trajectory* $\mathbf{p_d}$ *for all* $\mathbf{x_{out}}$.

Proof From Theorem 1, the closed-loop tracking system (40) that results from applying the feedback defined by (37) and (39) to the outer-loop dynamics is exponentially stable for all $\mathbf{x_{out}}$ and for all $\boldsymbol{\eta}$ satisfying $|\varphi| < \frac{\pi}{2}$ and $|\theta| < \frac{\pi}{2}$. Once the *zero dynamics* are defined by $\dot{\mathbf{x}}_\mathbf{out} = f(\mathbf{x_{out}}, \mathbf{0})$, the conditions regarding the Euler angles are always satisfied. Therefore, the referred zero dynamics globally exponentially track $\mathbf{p_d}$ for all $\mathbf{x_{out}}$. □

The control strategy is schematized in Fig. 3. Whereas the position and yaw references are defined by the user, the outer-loop control determines the required thrust direction and thus defines the pitch and roll angles references, θ_d and φ_d, respectively. In this direction, the vector $\mathbf{u_{out}}$ is redefined as follows:

$$\mathbf{u_{out}} = (\cos(\varphi_d)\sin(\theta_d), \sin(\varphi_d)) \tag{42}$$

Consequently, the system (33) reshapes into

$$\dot{\mathbf{x}}_{out} = \begin{bmatrix} \mathbf{0} & \boldsymbol{I}_2 \\ \mathbf{0} & \mathbf{0} \end{bmatrix}\mathbf{x_{out}} + g\begin{bmatrix} \mathbf{0} & \mathbf{0} \\ \cos\psi & \sin\psi \\ \sin\psi & -\cos\psi \end{bmatrix}\mathbf{u_{out}} + \begin{bmatrix} \mathbf{0} \\ \boldsymbol{\Gamma} \end{bmatrix} \tag{43}$$

where $\boldsymbol{\Gamma} \in \mathbb{R}^2$ corresponds to the interconnection term of the horizontal movement dynamics that results from the attitude tracking error and is given by:

$$\boldsymbol{\Gamma} = g\begin{bmatrix} \cos\psi & \sin\psi \\ \sin\psi & -\cos\psi \end{bmatrix}\left(\begin{bmatrix} \cos(\varphi)\sin(\theta) \\ \sin(\varphi) \end{bmatrix} - \mathbf{u_{out}}\right) \tag{44}$$

Note that this term is bounded by

$$\|\boldsymbol{\Gamma}\| \leq 2g\sqrt{2} \tag{45}$$

Further, the tracking system for the zero dynamics, first presented in (40), reshapes into

$$\begin{bmatrix} \mathbf{e_1}^\top\ddot{\mathbf{e}}_p \\ \mathbf{e_2}^\top\ddot{\mathbf{e}}_p \end{bmatrix} = \begin{bmatrix} \mathbf{e_1}^\top(-k_{i_x}\boldsymbol{\zeta}_\mathbf{p} - k_x\mathbf{e_p} - k_{\dot{x}}\dot{\mathbf{e}}_p) \\ \mathbf{e_2}^\top(-k_{i_y}\boldsymbol{\zeta}_\mathbf{p} - k_y\mathbf{e_p} - k_{\dot{y}}\dot{\mathbf{e}}_p) \end{bmatrix} + \boldsymbol{\Gamma} \tag{46}$$

Bearing in mind (42), the references φ_d and θ_d are extracted from the control law vector $\mathbf{u_{out}}$ through the following expressions:

$$\varphi_d = \sigma(\arcsin(\mathbf{u_{out}}_2)) \tag{47}$$

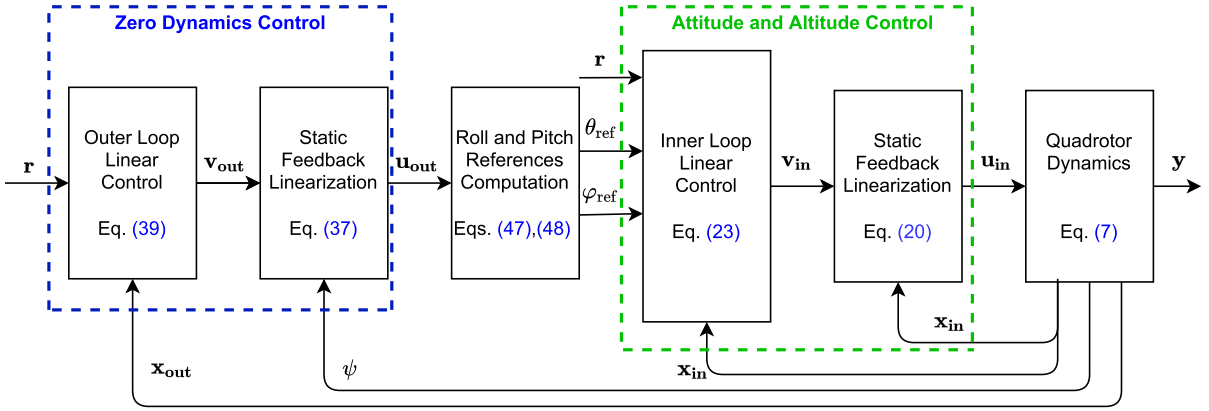

Fig. 3 Scheme of the proposed control solution

$$\theta_d = \arcsin\left(\frac{\mathbf{u_{out}}_1}{\cos\left(\arcsin\left(\mathbf{u_{out}}_2\right)\right)}\right) \tag{48}$$

Theorem 2 *Consider the closed-loop system comprised of the nonlinear system* (7) *and the input-output linearizing controller defined by* (20) *and* (23)*. Consider the local diffeomorphism described in* (22)*. Let the remaining dynamics, corresponding to the horizontal movement dynamics* (33)*, be input-output linearized and controlled through* (37) *and* (39)*. The resulting closed-loop tracking system system is regionally asymptotically stable.*

Proof From [15, Theorem 3], one states that the application of the input-output linearizing controller, defined by (20) and (23), and the local diffeomorphism expressed in (22) to the system (7) while considering the output vector (19) yields the closed-loop (25), which comprises the altitude and attitude tracking dynamics, that guarantees asymptotic convergence of the state-variables $\boldsymbol{\eta}$ to the desired $\boldsymbol{\eta_d}$ for $|\varphi| < \frac{\pi}{2}$ and $|\theta| < \frac{\pi}{2}$. Once the nonlinear system (7) comprehends 12 state-variables and the sum of the entries of the relative degree vector for the output (19) is equal to 8, exists an unobservable subsystem, characterized by the dynamics associated with the remaining 4 state-variables, that corresponds to the horizontal movement dynamics expressed in (33) and (34). The interaction between the inner-loop dynamics and the horizontal movement corresponds to a cascade system with the following form:

$$\dot{\mathbf{x}}_{\mathbf{out}} = f\left(\mathbf{x}_{\mathbf{out}}, \mathbf{x}_{\mathbf{in}}\right), \quad \dot{\mathbf{x}}_{\mathbf{in}} = h\left(\mathbf{x}_{\mathbf{in}}\right) \tag{49}$$

Since the only state-variables entering the outer-loop from the inner-loop are the Euler angles, the former equations can be rewritten as

$$\dot{\mathbf{x}}_{\mathbf{out}} = f\left(\mathbf{x}_{\mathbf{out}}, \boldsymbol{\eta}\right), \quad \dot{\mathbf{x}}_{\mathbf{in}} = h\left(\mathbf{x}_{\mathbf{in}}\right) \tag{50}$$

Consider the outer-loop dynamics given by (43). In the absence of the input $\boldsymbol{\Gamma}$, which models the impact of the attitude tracking error on the outer-loop dynamics, it follows from Theorem 1 that the outer-loop dynamics, with the definition of the input vector (32) and the output vector (34), are input-output linearized and controlled through the feedback expressed by (37) and (39). As a result, the closed-loop tracking system (46), in the absence of the input $\boldsymbol{\Gamma}$, i.e., $\boldsymbol{\Gamma} = \mathbf{0}$, is exponentially stable for any initial state state $\mathbf{x_{out}}(0)$, ensuring, thereby, the exponential convergence of the state-variables $\mathbf{x_{out}}$ to the desired trajectory $\mathbf{p_d}$. According to [25, section 2.6], since the characteristic polynomial of each resulting chain of integrators of the tracking system (40) is Hurwitz, the resulting tracking system (43) is input-to-state stable. Consequently, a bounded input $\boldsymbol{\Gamma}$ results in bounded state trajectories and $\boldsymbol{\Gamma}$ converging to zero imply the outer-loop tracking errors converging to zero. From (45), one has that the input $\boldsymbol{\Gamma}$ is bounded. Furthermore, from the inner-loop control, the state-variables $\boldsymbol{\eta}$ asymptotically converge to the desired $\boldsymbol{\eta_d}$ for $|\varphi| < \frac{\pi}{2}$ and $|\theta| < \frac{\pi}{2}$. Hence, $\boldsymbol{\Gamma} \to \mathbf{0}$ for $t \to \infty$. Moreover, from Corolary 1, the *zero dynamics*, defined by $\dot{\mathbf{x}}_{\mathbf{out}} = f\left(\mathbf{x}_{\mathbf{out}}, \mathbf{0}\right)$, globally exponentially track the desired trajectory $\mathbf{p_d}$ for all $\mathbf{x_{out}}$. Thus, following the Theorem enunciated in [26], the resulting cascade system (50) asymptotically

converges to $(\mathbf{p}, \boldsymbol{\eta}) = (\mathbf{0}, \mathbf{0})$ provided that $|\varphi| < \frac{\pi}{2}$ and $|\theta| < \frac{\pi}{2}$. Consequently, the closed-loop tracking system that results from applying the input-output linearizing controller defined by (20) and (23), the *local diffeomorphism* described in (22) and the input-output linearizing controller expressed in (37) and (39) to the nonlinear system (7) is asymptotically stable for all $\mathbf{x}$ that satisfies the conditions $|\varphi| < \frac{\pi}{2}$ and $|\theta| < \frac{\pi}{2}$. □

When compared to the solution reported in [15], the outer-loop control law devised, based on Feedback Linearization, enables extending the region of asymptotic stability from the origin to all the points $\mathbf{x}$ satisfying the conditions $|\varphi| < \frac{\pi}{2}$ and $|\theta| < \frac{\pi}{2}$. In this way, the state-space region with proven asymptotic stability yields a very comprehensive flight envelope. The most frequent quadrotor applications, namely monitoring, inspection, and surveillance, are circumscribed to a smaller flight envelope. Regarding single-loop solutions based on dynamic feedback linearization, the input-output linearizing control law, $\mathbf{u} = -\Lambda^{-1}(\mathbf{x})\,\mathbf{b}(\mathbf{x}) + \Lambda^{-1}(\mathbf{x})\,\mathbf{v}$, is derived from the fourth-order time derivative of the position. Thus, bearing in mind the quadrotor dynamic model, the resulting decoupling matrix Λ and the vector $\mathbf{b}$ require a large number of computations. Furthermore, the decoupling matrix is singular for null thrust values, in addition to the cases when $|\theta| = \frac{\pi}{2}$ or $|\varphi| = \frac{\pi}{2}$ [11]. Moreover, the single-loop solutions reported in the literature do not incorporate any integral action in the architecture. On the other hand, the strategy proposed by the authors has integral action embedded in both loops, which enables dealing more effectively with constant disturbances and parameter variations.

4 Simulation

A simulation model of the quadcopter was developed in furtherance of studying the approach and assessing its potential beforehand. The prior validation is indeed crucial for analyzing the impact of uncertainties and external disturbances that might significantly affect the closed-loop behavior. The actuators model was considered through the inclusion of the motor mixing, described by (4), and the computation of the PWM commands, based on the experimentally determined equations reported in [27, Appendix A]. In this way, the simulation comprehends the limitations imposed by saturation as follows: the thurst T and moments $\boldsymbol{\tau}$ required to track the references are determined by control law; posteriorly, by resorting to the motor mixing equation, the thrust force T_i that each actuator has to provide is calculated; finally, using the referred experimental relations, the PWM commands for each rotor, ranging from 0 to 100 %, are obtained. Note that the saturation is only applied to the PWM commands. To further approximate the simulation to the real quadcopter, noise disturbances, modeled as zero-mean Gaussian white noise with the variances being determined from real sensory data, were included as well. The selected sampling time for the simulation was 0.01 seconds. The relevant physical quantities of the quadcopter consider in the simulation are detailed in Table 1.

Table 1 Important physical quantities of the quadcopter considered in the simulation model

L[m]	m [kg]	I_x[kg m^2]	I_y[kg m^2]	I_z[kg m^2]
0.127	0.460	2.24×10^{-3}	2.90×10^{-3}	5.30×10^{-3}

Concerning the design parameters, the aim was at position responses with a maximum overshoot lower than 2 %, a settling time lower than 5 seconds, and without static error. Given the crucial role of the rotational responses in the stabilization of the quadcopter [16], faster angular responses are mandatory to cope with the references that result from the outer loop control. Thus, the pitch and roll angles step responses should present a settling time lower than 1 second. With respect to the yaw angle response, once the definition of its reference is independent of the outer-loop control, it is not required to establish a settling time requirement as demanding. Thereby, for the latter, a settling time lower than 3 seconds is reasonable. Furthermore, it was shown, in [28], that an aggressive yaw control can easily lead to saturation of multiple actuators, especially when commanding large yaw changes, and, consequently, affect the control performance. Regarding the overshoot and the static error, the angular responses should fulfill the same requirements established for the position responses. The $\mathbf{Q}^*$ and $\mathbf{R}^*$ matrices used in the several control channels are detailed in Table 2. To prevent a scenario in which the conditions $|\varphi| < \frac{\pi}{2}$ and $|\theta| < \frac{\pi}{2}$ are violated, the initial attitude is set in accordance with this bounds. In addition, to avoid the generation of angular references φ_d and θ_d that can result in the inner-loop operating in the vicinity of singularities, a smooth saturation function with a saturation level of less than $\frac{\pi}{2}$ is applied to both φ_d and θ_d.

Table 2 $\mathbf{Q}^*$ and $\mathbf{R}^*$ matrices used in the optimal gains computation for each subsystem of the control approach

Subsystem	$\mathbf{Q}^*$	$\mathbf{R}^*$
φ	$\text{diag}(6 \times 10^4, 7.5 \times 10^2, 2 \times 10^6)$	1
θ	$\text{diag}(6 \times 10^4, 7.5 \times 10^2, 2 \times 10^6)$	1
ψ	$\text{diag}(7.5 \times 10^3, 50, 1 \times 10^5)$	1
x	$\text{diag}(6, 1 \times 10^{-3}, 30)$	25
y	$\text{diag}(6, 1 \times 10^{-3}, 30)$	25
z	$\text{diag}(30, 1, 85)$	1

Table 3 Cases evaluated in the model parameters variation test

Case	c_m	c_I
1	0.50	0.25
2	0.50	4.00
3	1.50	0.25
4	1.50	4.00

To ascertain the performance of the proposed control and its model dependency, the impact of considering inaccurate values of the mass and the inertia of the quadcopter is studied. Additionally, the robustness of the control system against an external force is evaluated. Let $\bar{m}$ and $\bar{\mathbf{I}} = \text{diag}\left(I_x,\ I_y,\ I_z\right)$ represent the nominal values detailed in Table 1 and $\tilde{m}$ and $\tilde{\mathbf{I}}$ denote percentages of these values that are computed through the following expressions:

$$\tilde{m} = c_m \bar{m} \tag{51}$$

$$\tilde{\mathbf{I}} = c_I \bar{\mathbf{I}} \tag{52}$$

The control strategy was evaluated considering four different cases of simultaneous significant deviations in the mass and inertia values. These cases are summarized in Table 3. The references for the horizontal position and for the altitude are steps with an amplitude of 3 and 2 m, respectively, and the reference for the yaw angle is a ramp with a slope of 0.1 rad s^{-1}. After 60 seconds, the system is subjected to an external force of $1N$, applied with the inertial y axis positive direction.

The position and yaw angle responses obtained in the model parameters variation test with the nonlinear control architecture proposed are depicted in Fig. 4. These are very promising and important results since the performance did not deteriorate significantly even tough significant changes in the model parameters were simultaneously considered, an external force was

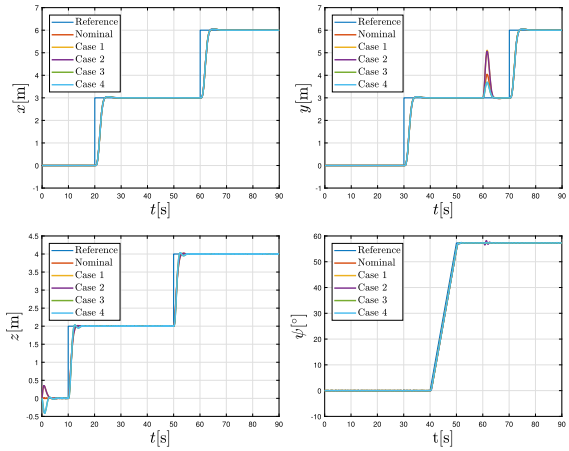

Fig. 4 Responses obtained with the nonlinear control approach in the parameters variation test. From left to right, top to bottom: **a** x inertial; **b** y inertial; **c** Height; **d** Yaw angle

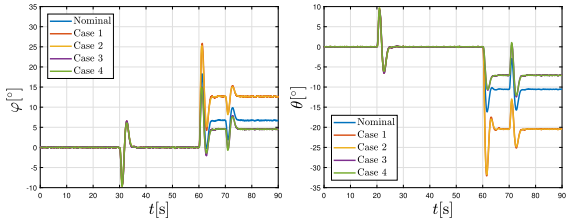

Fig. 5 Roll and Pitch angles obtained in the parameters variation test. From left to right: **a** Roll; **b** Pitch

applied, and the amplitude of the steps required aggressive responses. Not only the responses remained stable, but also the control performance presented a consistency throughout the tests, which is reflected in the fact that the responses respected the design criteria. The integral action plays a major role in diminishing the model dependence and in enhancing the performance of the control architecture [27]. The pitch and roll angles verified in this test are displayed in Fig. 5. It is noticeable that the two Euler angles did not present relevant variations, from case to case, throughout the first 60 seconds. After that, the effect of the constant external force is evident. As expected, the cases in which a smaller mass is considered present, in modulus, angular responses with higher values since this force results in a higher acceleration.

The actuation, in terms of thrust and moments, generated during the parameters variation test is depicted in Fig. 6. Predictably, the higher mass cases required higher thrust values to perform the trajectory. From the external force application at 60 seconds stems the

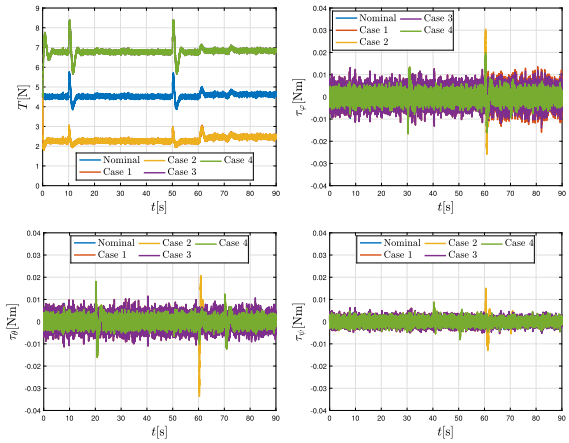

Fig. 6 Thurst and Moments obtained in the parameters variation test. From left to right, top to bottom: **a** Thrust; **b** Roll Moment; **c** Pitch Moment; **d** Yaw Moment

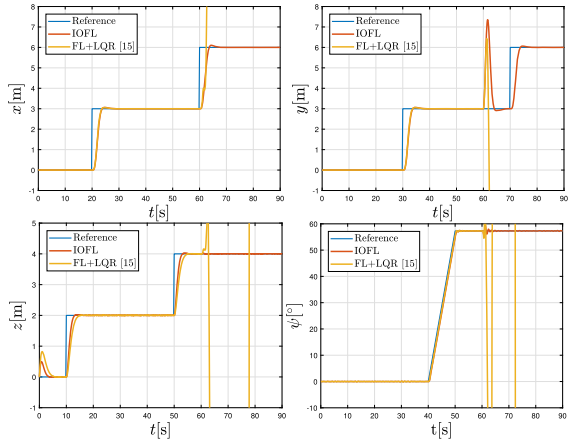

Fig. 7 Responses obtained with the nonlinear control approach and the strategy reported in [15] for $c_m = 0.25$ and $c_I = 4$. From left to right, top to bottom: **a** x inertial; **b** y inertial; **c** Height; **d** Yaw angle

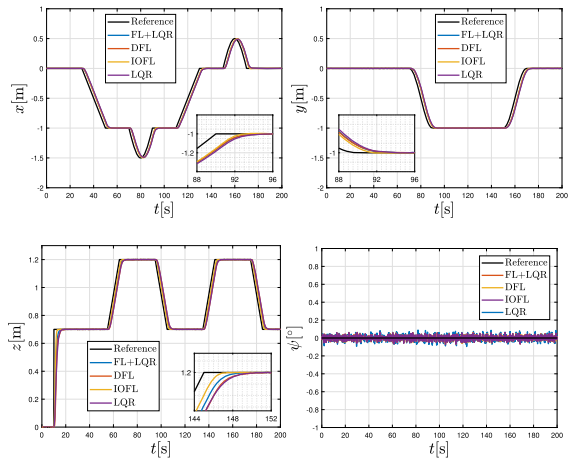

Fig. 8 Responses obtained during trajectory tracking in simulation with the nonlinear control approach developed and comparable strategies found in the literature. From left to right, top to bottom: **a** x inertial; **b** y inertial; **c** height; **d** yaw angle

higher moment values verified during the test. In particular, case 3 displays the higher moments values since it conjugates the smaller mass and higher inertia, which translates into being more affected by the external force and requiring a higher actuation value to overcome it.

To illustrate the improved performance of the novel control solution compared to the previous approach developed by the authors, [15], an additional case, with $c_m = 0.25$ and $c_I = 4$, was simulated. The responses obtained with both solutions are presented in Fig. 7. The novel control solution recovered the desired reference after being impacted by the external force of 1N. On the other hand, the approach reported in [15] presented an unstable behavior when subjected to the external force. Hence, the underlying improvement of the new control strategy translates into a higher degree of robustness.

To evaluate the capacity of the proposed control solution to follow a predefined trajectory, one was created and given as reference. This trajectory, excluding the take-off, is formed by rectilinear and semicircular sections with constant linear and angular velocities, respectively, and is defined with a constant yaw angle equal to zero. To the end of confronting the proposed control solution performance with strategies found in the literature relying on Feedback Linearization or Linear Quadratic Regulator techniques, simulation responses obtained with these comparable strategies are presented as well.

In Fig. 8, the simulation results attained with the proposed methodology (IOFL) are displayed in conjunction with the responses obtained with the following strategies from the literature: double-loop solution resulting from applying the LQR technique to the linearized model [17] (LQR); double-loop architecture in which a static feedback linearization control law governs the attitude and altitude dynamics, and the linearized zero dynamics are rendered stable by employing the LQR method (FL+LQR) [15]; single-loop control structure based on Feedback Linearization with dynamic extension (DFL) [12]. From the referred figure, it can be concluded that the strategies yielded a suc-

Table 4 Root-mean-square error obtained in simulation with the proposed nonlinear control approach and comparable strategies from the literature

Strategy	x [m]	y [m]	z [m]	ψ [°]
LQR [17]	0.0814	0.0633	0.0479	0.0302
FL+LQR [15]	0.0742	0.0576	0.0385	0.0216
DFL [12]	0.0729	0.0566	0.0484	0.0216
IOFL	0.0688	0.0525	0.0270	0.0216

cessful following of the desired trajectory. Concerning the yaw angle time response, the methodology fulfills the objective.

In order to facilitate comparison, the root-mean-square error obtained with each control solution tested is detailed in Table 4. It is noticeable that the control approach devised attained smaller position and yaw angle root-mean-square error values. Hence, the proposed solution performed better than the comparable strategies found in the literature.

5 Implementation

The commercially available Parrot AR. Drone 2.0 was used to validate the devised control architecture. The referred vehicle possesses a 3-axis accelerometer, a 3-axis gyroscope, a barometric pressure sensor, two ultrasonic transducers, and a 3-axis compass. These sensors measure the altitude, acceleration, angular velocity, and magnetic field of the quadcopter. The Parrot AR. Drone 2.0 generates thrust through brushless motors. These motors are controlled by feeding PWM commands, corresponding to the percentage of the full speed of the rotor, computed from the control law through experimentally determined relations. For further details concerning this computation, see [15].

In furtherance of implementing the control approach in the quadrotor, the "AR Drone 2.0 Quadcopter Embedded Coder" [29] was used. This *Simulink* project provides direct access to the sensors and the actuators of the quadcopter. In Fig. 9, the connections established between the computer running the motion capture system *Qualisys*, the host computer, where the *Simulink* model is compiled, and the hardware board of the UAV, where the control and estimation computations are performed, are summarized. The computer where the *Qualisys* is running transmits the data to the

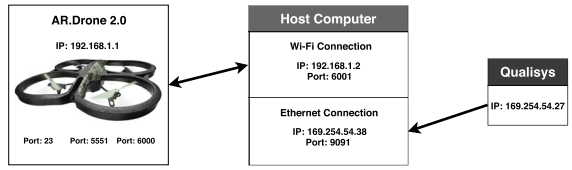

Fig. 9 Network Diagram describing the connections between the computer running the Qualisys Track Manager, the host computer and the UAV

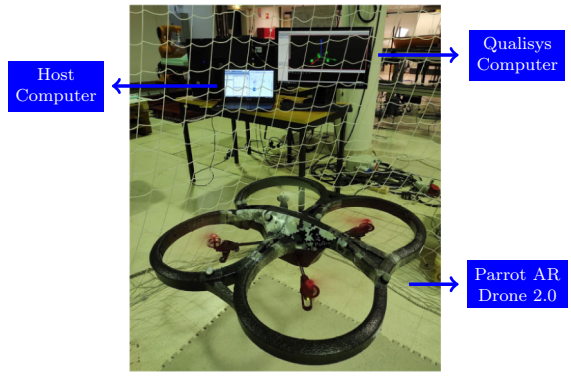

Fig. 10 Experimental setup

host computer through an ethernet cable using the User Datagram Protocol (UDP). The data received is sent through a Wi-Fi connection, also using UDP, to the quadrotor. The *Simulink* model is compiled to C-Code and a binary file, executable on the quadrotor operating system, is generated and deployed to its hardware board. A wireless File Transfer Protocol (FTP) connection assures the deployment. Additional UDP connections are configured to communicate in real-time with the generated code deployed running in the quadrotor board.

For attitude estimation, the nonlinear filter developed by Madeiras et al. [30] was used. This filter fuses the accelerometer and gyroscope measurements and is proved to be uniformly asymptotically stable assuming a bounded pitch angle ($|\theta| < \pi/2$). The linear velocities were estimated by resorting to a Kalman Filter as described in [27]. The inner-outer loop control architecture and the estimation solution were implemented with a sampling time of 0.01 seconds. The experimental setup is depicted in Fig. 10.

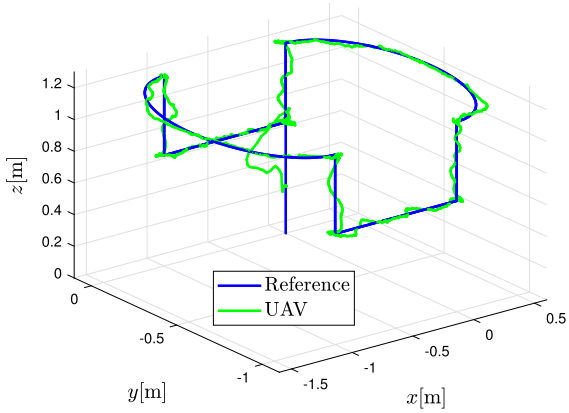

Fig. 11 Trajectory tracking in 3D space obtained with the nonlinear control solution

6 Experimental Results

The first experimental test consists of evaluating the capacity of performing a predefined trajectory identical to the one tested in simulation. Comparisons between the experimental and the simulation responses are drawn.

Implementing the control structure based on the Feedback Linearization technique with *zero dynamics* stabilization led to the experimental results that are exhibited in Fig. 11. By observing this figure, one notices the success attained by the proposed approach in tracking the trajectory. It is relevant to highlight the inclusion of the take-off in the results displayed and the fact of the altimeter not measuring heights inferior to 0.30m. Furthermore, it is worth pointing out the use of a heavier battery. Notwithstanding this change in the total mass of the quadrotor, the integral action included was able to overcome it, which led to a good performance.

The transition of the controllers from the simulation design to the validation with the actual quadcopter was managed by conducting hovering and step responses tests prior to the trajectory tracking experiment. Whereas the attitude and altitude controllers designed in simulation led to a behavior that fulfilled the objectives, the outer-loop controllers had to be adjusted. The matrices $\mathbf{Q}^*$ and $\mathbf{R}^*$ used in this adjustment are detailed in Table 5.

Simulations responses for trajectory tracking were obtained with these new controllers in furtherance of comparing with the experimental results. In Fig. 12, the

Table 5 $\mathbf{Q}^*$ and $\mathbf{R}^*$ matrices used in the controllers adjustment

Subsystem	$\mathbf{Q}^*$	$\mathbf{R}^*$
x	$\text{diag}(10, 1 \times 10^{-2}, 40)$	30
y	$\text{diag}(10, 1 \times 10^{-2}, 40)$	30

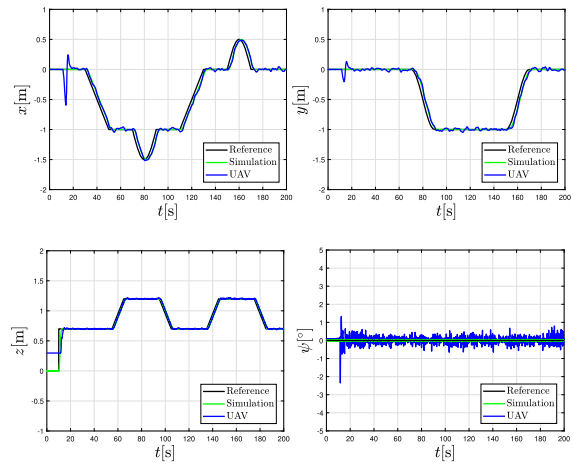

Fig. 12 Responses obtained with the quadrotor during trajectory tracking with the proposed nonlinear control approach. From left to right, top to bottom: **a** x inertial; **b** y inertial; **c** Height; **d** Yaw

simulation and experimental responses are depicted. From the observation of this figure, one concludes that the control solution proposed allows a good following of the trajectory. The similarities between the simulation and the experimental results evidence the proximity between the nonlinear model developed and the actual system. The higher deviations visible in the x and y responses, corresponding to the maximum error obtained, stem from the horizontal drift verified during the take-off. This drift occurs since the outer-loop control is only activated once the vehicle is at an altitude superior to 0.60 m. Excluding the take-off, the experimental response does not deviate more than 5 cm from the simulated response. A continuous oscillation caused by high-order effects, which were discarded in simulation, is verified in the experiment. Its small amplitude legitimates the high-order effects neglect in the quadrotor model construction.

The roll and pitch angles references generated by the outer-loop control and the estimates obtained during the take-off and the following of the trajectory are depicted in Fig. 13. It is noticeable that these angles presented reduced values during the experimental test.

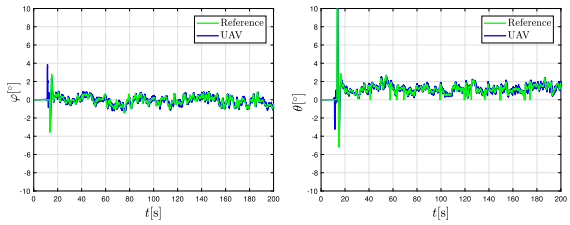

Fig. 13 Roll and pitch angles references generated and the respective responses obtained during trajectory tracking in experimental test using the nonlinear control approach. From left to right: **a** Roll; **b** Pitch

The sudden variations in the first twenty seconds result from offsetting the positional drift that arises during the take-off. Moreover, the inner-loop capacity to cope with the references generated by the *zero dynamics* control is demonstrated by the responses displayed in this figure. By embarking on a more detailed analysis, unexpected zero-value references are detected, especially on the right graph. The outer-loop control is deactivated whenever the communication with the motion capture system fails. In these situations, the angular references are set to zero, which leads to these unexpected values and, subsequently, to x and y deviations. As a consequence, the error increases.

The thrust force and moments computed by the control structure are shown in Fig. 14. The heavier battery used led to higher values of thrust. Regarding the moments, the higher values were required when the position control was activated, since the quadcopter had to compensate for the positional drift that occurred during the take-off. Throughout the tracking, due to the trajectory not being aggressive, the actuation did not present abrupt variations.

The transformed-input vectors v_{in} and v_{out} computed during the take-off and trajectory tracking are exhibited in Fig. 15.

From Fig. 16, where the PWM commands are displayed, one notes that the actuation did not saturate during the take-off and the trajectory tracking.

In Table 6, the trajectory tracking root-mean-square error obtained in simulation and with the real system is detailed. The experimental validation values are close to the ones obtained in simulation, with particular emphasis on the height response that presented approximately the same error. Concerning the other outputs, the error increased with the transition to the actual UAV, which was predictable since higher-order dynam-

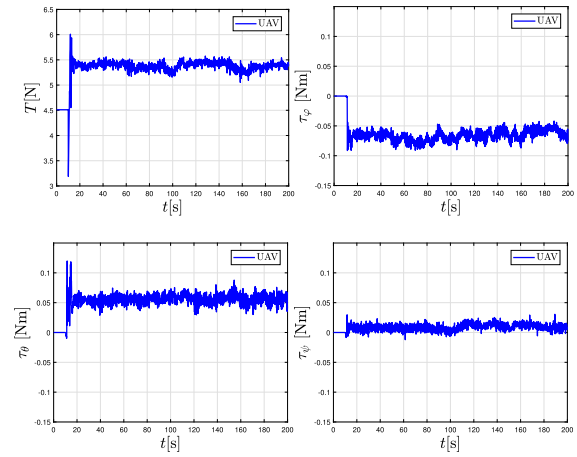

Fig. 14 Thrust and Moments computed during the trajectory tracking with the proposed nonlinear control approach. From left to right, top to bottom: **a** Thrust; **b** Roll Moment; **c** Pitch Moment; **d** Yaw Moment

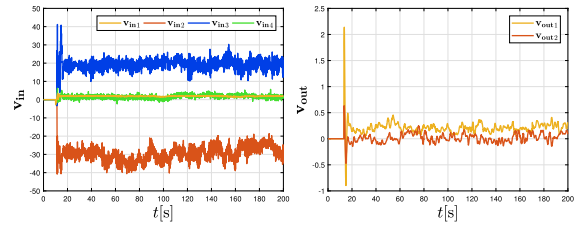

Fig. 15 Transformed-inputs computed during trajectory tracking in experimental test using the nonlinear control approach. From left to right: **a** Inner-Loop; **b** Outer-Loop

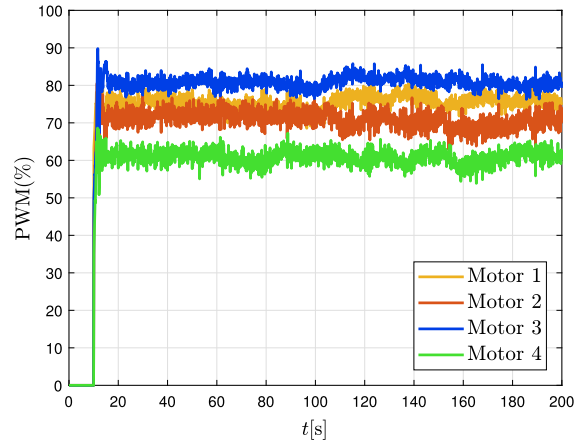

Fig. 16 PWM Commands computed during trajectory tracking with the nonlinear control approach

ics effects were discarded in the model considered. The root-mean-square error obtained for the inertial coor-

Table 6 Root-mean-square error obtained in simulation and in the experimental test with the proposed nonlinear control approach

	x [m]	y [m]	z [m]	ψ [°]
Simulation	0.0688	0.0525	0.0270	0.0216
Experimental	0.0706	0.0583	0.0272	0.1889

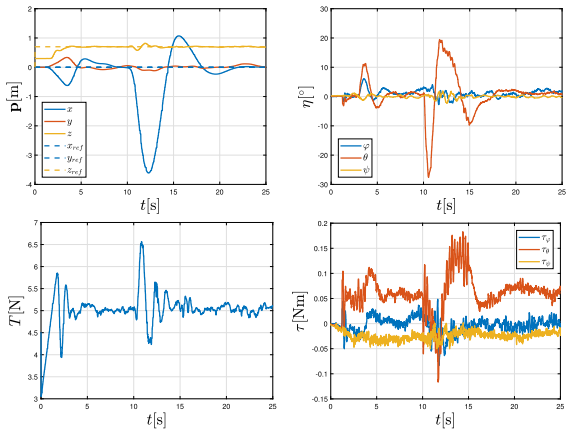

Fig. 17 Responses obtained in the second experiment. From left to right, top to bottom: **(a)** Position; **(b)** Euler Angles; **(c)** Thrust; **(d)** Moments

dinates is mostly due to the static error in the following of ramp inputs. Furthermore, the inertial coordinate x, once is the subsystem more subjected to this type of reference, presents the higher value of root-mean-square error. Nonetheless, the errors obtained are reduced and validate the control strategy proposed.

In furtherance of deepening the study, the behavior of the control solution when performing aggressive maneuvers and when subjected to considerable constant perturbations is evaluated. To this end, an experiment, consisting of suddenly applying an offset of $-35°$ to the pitch reference generated by the outer-loop while the quadrotor is hovering, was carried out. The results obtained in this experiment are displayed in Fig. 17. Despite the significant unexpected constant perturbation and the consequent aggressive maneuver, which solicited the nonlinear dynamics of the quadrotor, the vehicle presents a stable response and returns to the desired position. The integral action embedded in both loops is indeed crucial for the control strategy to deal effectively with unexpected significant constant perturbations. A video of this experiment is available in https://www.youtube.com/watch?v=B0J3SmaxQS0.

7 Conclusion

An inner-outer loop control structure, with proof of asymptotic stability for $|\varphi| < \frac{\pi}{2}$ and $|\theta| < \frac{\pi}{2}$, was devised, relying twice on the nonlinear technique Feedback Linearization in combination with LQR control with integral action, and successfully validated not only in simulation but also experimentally.

In the simulation, the proposed control solution handled combined significant deviations in the mass and inertia values, even when subjected to a constant external force, without considerably affecting its responses. The solution potential was also evaluated for trajectory tracking, having performed favorably compared to other strategies from the literature that rely on the same control methods applied.

The solution was successfully implemented on an off-the-shelf quadrotor. The results obtained in trajectory tracking validated the proposed strategy and, given the manifest similarities between the attained responses with the actual aerial vehicle and in simulation, evidenced the satisfactory degree of accuracy of the model considered. The second test conducted further emphasized the importance of the integral action: besides decreasing the model dependency of the control structure, as demonstrated in simulation, this action also allows overcoming significant constant perturbations. The latter experiment evidenced the stable behavior of the control system when performing more aggressive maneuvers.

Acknowledgements This work was supported by FCT, through IDMEC, under LAETA, project UIDB/50022/2020. L. Martins holds a scholarship from the FCT project DECENTER [LISBOA-01-0145-FEDER-029605], funded by the Lisboa 2020 and PIDDAC programs.

Code availability Not applicable.

Declarations

Conflict of interest The authors declare that they have no conflict of interest.

References

1. Kabiri, M., Atrianfar, H., Menhaj, M.B.: Trajec-tory tracking of a class of under-actuated thrust-propelled vehicle with uncertainties and unknown disturbances. Nonlinear Dyn. **90**, 1695–1706 (2017)

2. Hou, Z., Lu, P., Tu, Z.: Nonsingular terminal sliding mode control for a quadrotor UAV with a total rotor failure. Aerosp. Sci. Technol. **98**, 105716 (2020)
3. Wang, B., Yu, X., Mu, L., Zhang, Y.: A dual adaptive fault-tolerant control for a quadrotor helicopter against actuator faults and model uncertainties without overestimation. Aerosp. Sci. Technol. **99**, 105744 (2020)
4. Zhao, Z., Cao, D., Yang, J., Wang, H.: High-order sliding mode observer-based trajectory tracking control for a quadrotor UAV with uncertain dynamics. Nonlinear Dyn. **102**, 2583–2596 (2020)
5. Li, C., Zhang, Y., Li, P.: Full control of a quadrotor using parameter-scheduled backstepping method: implementation and experimental tests. Nonlinear Dyn. **89**, 1259–1278 (2017)
6. Glida, H.E., Abdou, L., Chelihi, A., Sentouh, C., et al.: Optimal model-free backstepping control for a quadrotor helicopter. Nonlinear Dyn. **100**, 3449–3468 (2020)
7. Martins, L., Cardeira, C., Oliveira, P.: Global Trajectory Tracking for Quadrotors: An MRP-Based Hybrid Backstepping Strategy In: 2021 60th IEEE Conference on Decision and Control (CDC) (2021), 5759-5764
8. Eskandarpour, A., Sharf, I.: A constrained errorbased MPC for path following of quadrotor with stability analysis. Nonlinear Dyn. **99**, 899–918 (2020)
9. Freddi, A., Lanzon, A., Longhi, S.: A feedback linearization approach to fault tolerance in quadrotor vehicles. IFAC Proc. **44**, 5413–5418 (2011)
10. Wang, J. et al. Attitude Free Position Control of a Quadcopter Using Dynamic Inversion. Infotech @ Aerospace 2011 (2011)
11. Roza, A., Maggiore, M.: Path Following Controller for a Quadrotor Helicopter In: 2012 American Control Conference (ACC) (2012), 4655-466
12. Bonna, R., Camino, J.: Trajectory Tracking Control of a Quadrotor Using Feedback Linearization In: International Symposium on Dynamic Problems of Mechanics (2015)
13. Vallejo-Alarcon, M.A.: Robust backstepping control for highly demanding quadrotor flight. J. Control Eng. Appl. Inform. **22**, 51–62 (2020)
14. Aboudonia, A., El-Badawy, A., Rashad, R.: Disturbance observer-based feedback linearization control of an unmanned quadrotor helicopter Proceedings of the Institution of Mechanical Engineers, Part I. J. Syst. Control Eng. **230**, 877–891 (2016)
15. Martins, L., Cardeira, C., Oliveira, P.: Feedback Linearization with Zero Dynamics Stabilization for Quadrotor Control. J. Intell. & Robotic Syst. **101**, 1–17 (2021)
16. Mayhew, C.G., Sanfelice, R.G., Teel, A.R.: Quaternion-Based Hybrid Control for Robust Global Attitude Tracking. IEEE Trans. Autom. Control **56**, 2555–2566 (2011)
17. Martins, L., Cardeira, C., Oliveira, P.: Linear Quadratic Regulator for Trajectory Tracking of a Quadrotor. IFAC-PapersOnLine 52. In: 21st IFAC Symposium on Automatic Control in Aerospace ACA 2019, 176-181. issn: 2405-8963 (2019)
18. Stengel, R.: Optimal Control and Estimation (Dover Publications, 1994)
19. Das, A., Subbarao, K., Lewis, F.: Dynamic Inversion of Quadrotor with Zero-Dynamics Stabilization. In: 2008 IEEE International Conference on Control Applications (2008)
20. Leishman, J. G.: Principles of Helicopter Aerodynamics (Cambridge University Press, 2000)
21. Mahony, R., Kumar, V., Corke, P.: Multirotor aerial vehicles: modeling, estimation, and control of quadrotor. IEEE Robotics & Autom. Magaz. **19**, 20–32 (2012)
22. Oriolo, G., Sciavicco, L., Siciliano, B., Villani, L.: Robotics: Modelling, Planning and Control (Springer, 2010)
23. Henson, M., Seborg, D. E.: Nonlinear Process Control (Prentice Hall PTR, 1997)
24. Isidori, A.: Nonlinear Control Systems (Springer Verlag, 1995)
25. Sontag, E. D.: In Nonlinear and Optimal Control Theory 163-220 (Springer, 2008)
26. Sontag, E. D.: Remarks on Stabilization and Input to-State Stability. In: Proceedings of the 28th IEEE Conference on Decision and Control **2**, 1376-1378 (1989)
27. Martins, L.: Linear and Nonlinear Control of UAVs: Design and Experimental Validation MA thesis. Instituto Superior Técnico, Lisbon, Portugal (2019)
28. Smeur, E., Höppener, D., De Wagter, C.: Prioritized Control Allocation for Quadrotors Subject to Saturation in (2017)
29. Lee, D.: AR.Drone 2.0 Support from Embedded Coder (2016) http://www.mathworks.com/hardware-support/ardrone.html
30. Madeiras, J., Cardeira, C., Oliveira, P.: Complementary Filter Vision-Aided for Attitude and Position Estimation: Design, Analysis and Experimental Validation. In: Proceedings of the 21st IFAC Symposium on Automatic Control in Aerospace (2019)